Earth Planets Space, **50**, 453–462, 1998

"Phobos events"—Signatures of solar wind interaction with a gas torus?

K. Baumgärtel[1,7], K. Sauer[2,7], E. Dubinin[2,3,7], V. Tarrasov[4,5,7], and M. Dougherty[6]

[1]*Astrophysikalisches Institut Potsdam, 14482 Potsdam, Germany*
[2]*Max-Planck-Institut für Aeronomie, 37191 Katlenburg-Lindau, Germany*
[3]*Institute of Space Research, 117810 Moscow, Russia*
[4]*Centre d'Etude des Environments Terrestre et Planetaires, 78140 Velizy, France*
[5]*Lviv Centre of the Institute of Space Research, 290601 Lviv, Ukraine*
[6]*Space and Atmospheric Physics, Imperial College, London SW72AZ, U.K.*
[7]*International Space Science Institute (ISSI), 3012 Bern, Switzerland*

(Received August 28, 1997; Revised January 30, 1998; Accepted February 20, 1998)

Following recent simulations of the Phobos dust belt formation (Krivov and Hamilton, 1997), the effective dust-induced charge density as estimated is too small to account for the significant solar wind (sw) plasma and magnetic field perturbations observed by the Phobos-2 spacecraft in 1989 near the crossings of the Phobos orbit. In this paper the sw interaction with the Phobos neutral gas torus is re-investigated in a two-ion plasma model in which the newly created ions are treated as unmagnetized, forming a beam (not a ring beam) in the sw frame. A linear instability analysis based on both a cold fluid and a kinetic approach shows that electromagnetic ion beam waves in the whistler range of frequencies, driven most unstable at oblique propagation and appearing as almost purely growing waves in the beam frame, aquire high growth rates and provide a likely mechanism to cause the observed events.

1. Introduction

In 1989, during its first three elliptical orbits around Mars, the Phobos-2 spacecraft observed significant plasma and magnetic field perturbations near the crossings of the orbit of the Martian moon Phobos (Riedler *et al*., 1989; see also Figs. 1 and 4). They have been suggested as giving indirect evidence for the presence of either a gas ring or a dust ring along the Phobos orbit (Dubinin *et al*., 1990; Ip and Banaskiewicz, 1990), but despite extensive theoretical work no satisfactory explanation of these remarkable observations has emerged. The existence of a Phobos dust torus was already postulated by Sloter in 1971, but it has to date not been directly observed. The possible presence of a gas ring with neutral number density exceeding that of the hot atomic oxygen background was pointed out by Ip and Banaskiewicz (1990) if a certain level of outgassing is maintained by the Phobos moon. Several studies have been performed in the past to shed light on the physical origin of the Phobos events, with major emphasis given to the sw-dust interaction. Russell *et al*. (1990) interpreted the events as usual forshock turbulence released by diffuse ions for situations where the spacecraft and the Martian bow shock are connected. Dubinin *et al*. (1995) suggested that the events are related to the pick-up of exospheric protons reflected from the bow shock. These models, however, cannot explain the coincidence of the events with the Phobos orbit crossings. Dubinin *et al*. (1991a, b) and Dubinin (1993) discussed qualitatively the possibility that a weakly outgassing Phobos as well as a dust ring may act as an obstacle to the sw. Krymski *et al*. (1992) carried out a more detailed qualitative study on the sw interaction with both the neutral gas halo and the dust torus and came to the conclusion that the observed magnetic and plasma perturbations do not result from the neutral gas because of too low a outgassing rate of Phobos and that the charged dust torus is most likely to be the source for the events. Sauer *et al*. (1993) and Baumgärtel and Sauer (1993) attempted an interpretation of the Phobos events in terms of whistler waves phase-standing upstream of the dust torus. In a continuation of this work, Baumgärtel *et al*. (1996) suggested that the events are signatures of crossings of a dispersed Mach cone supported by fast magnetosonic/whistler waves which are excited in response of the sw to a dust toroid with a disk-like cross section. Some of the features of the events could be explained in this model whereas several others remained unexplained.

The crucial parameter for any theory which ascribes the Phobos events to the Phobos dust torus is the magnitude of the total charge density established by the presence of charged dust grains of different size. Roughly speaking, the sw "feels" the dust only if its total charge density is not very small compared to the sw density (Baumgärtel and Sauer, 1992). In the Martian dayside environment, dust particles can be assumed to be positively charged, mainly due to solar uv radiation, at a potential of approximately 5 V regardless of their size (Horanyi *et al*., 1990). This implies that each dust grain may carry a large number of elementary charges. To estimate the total charge density, the particle density of dust grains of a specified size is required to be known. This knowledge is provided by a few of a number of simulation studies on the dynamics of dust ejecta from Phobos; a problem which attracted a great deal of interest in the past (Kholshevnikov *et al*., 1993; Ishimoto and Mukai, 1994; Krivov and Hamilton, 1997; a complete list of references

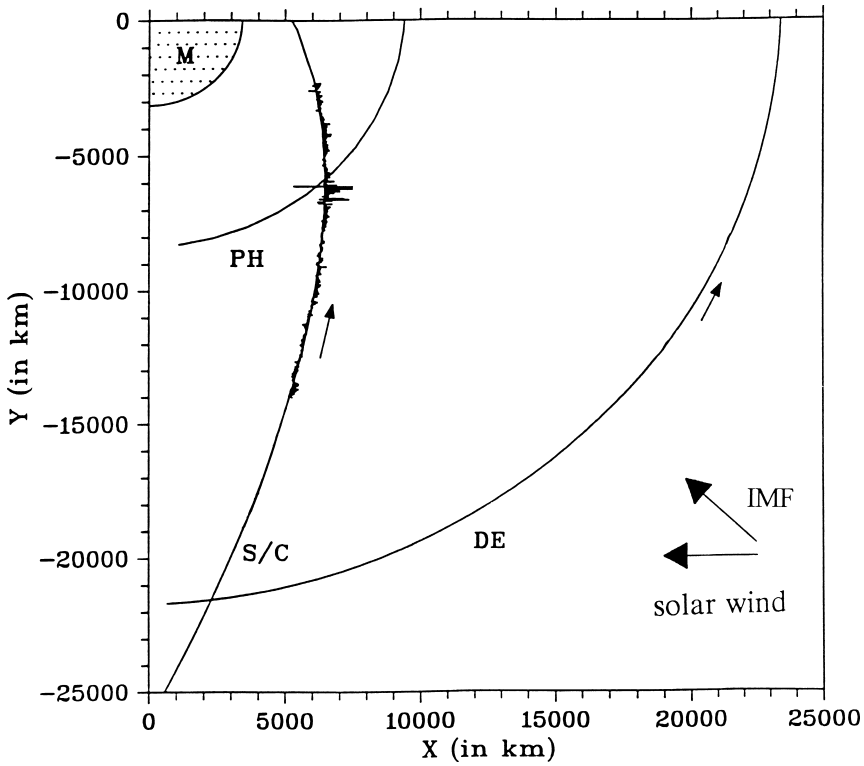

Fig. 1. Orbits of Martian moons Phobos (PH) and Deimos (DE) and spacecraft trajectory (S/C), projected onto the ecliptic *x*-*y*-plane. The deviation of the magnetic field magnitude *B* from its average value is attached to the spacecraft trajectory indicating the location of the event at the Phobos orbit crossing observed on Feb. 1, 1989.

can be found in the latest reference). Actually there is no commonly accepted estimate for the dust-induced charge density within the torus. The most recent simulation (Krivov and Hamilton, 1997) predicts densities of the order of 10^3 km^{-3} for particles sizes ranging from 10 μm–90 μm whereas a higher density of 10^5 km^{-3} is predicted for smaller grains of size 1 μm–10 μm. The charge Q of a spherical dust grain with radius a and potential V is given by the capacitance relation $Q = 4\pi\varepsilon_0 aV$. This yields the simple formula (Mendis and Axford, 1974)

$$Z = 700\phi\,(\mathrm{V})\; a\;(\mu\mathrm{m}) \qquad (1)$$

for the number Z of charges residing on a dust grain with radius a and Potential ϕ. Assuming a voltage of 5 V for each dust particle no matter what the size, we have $Z \approx 3.5 \times 10^4$ a (μm) and the above density estimate yields a total charge density of 3×10^9 km^{-3} = 3×10^{-6} cm^{-3}, which is six orders of magnitude smaller than the sw density. On the basis of these results, in spite of their possible uncertainty by two orders of magnitude, one can rule out the hypothesis that the Phobos events are caused by the Phobos dust torus. It is the purpose of this paper to re-investigate whether linear plasma instabilities of the sw interaction with a putative gas torus along the Phobos orbit can account for the observations, which would naturally explain the coincidence of the events with the crossings of the Phobos orbit.

We should finally mention that an event was additionally observed on Feb. 1, 1989 between the orbits of Phobos and Deimos, which thus can hardly be related to the dust/gas torus of any of the two moons. It was suggested (Sauer *et al.*, 1995) that this event can be attributed to Deimos itself which appears to be an effective obstacle to the sw. The particular position of Deimos to the spacecraft during the first elliptical orbit suggests an interpretation in terms of crossing of a fast wave Mach cone 15,000 km downstream of it.

2. Solar Wind Interaction with the Gas Torus

The two main sources for neutral gas in the Martian environment are the extended Martian exosphere and the emission of matter from the two Martian moons Phobos and Deimos. An early indication of possible outgassing from Deimos was found by Bogdanov (1981) who observed unusual sw disturbances far downstream in the wake of Deimos. In addition to outgassing, micrometerite impacts on the surface of the moons and—to a lesser extent—accretional interaction with the hot oxygen corona of Mars may contribute to the formation and maintainment of a neutral gas torus (Ip and Banaskiewicz, 1990). The presence of a heavy ion population with enhanced density near to the Phobos orbit may give rise to ion-ion beam instabilities, similar to those which are believed to operate in the sw interaction with cometary atmospheres (Wu and Davidson, 1972; Brinca and Tsurutani, 1987; Thorne and Tsurutani, 1987; Goldstein *et al.*, 1990; Brinca, 1991; Tsurutani, 1991; Gary, 1993). The basic mechanism is that new-born ions, created at a certain rate from the neutral gas, will be accelerated into cycloidal motion, forming a ring-beam like pitch angle distribution in the sw frame which is known to be highly unstable, giving rise to a variety of low frequency electromagnetic instabilities. Thereby, two distinct sources of free energy are provided, namely a field-aligned ion beam

and the gyrating ring distribution, both of which can lead to the excitation of plasma waves via resonant wave particle interaction. It depends on the cone angle α between the sw flow direction and the IMF which of these instabilities dominate. We emphasize, however, that unlike the cometary scenario, we are here confronted with a rather localized interaction region with a size of only a small fraction of the gyroradius of an exospheric ion (a sketch of the interaction scenario is depicted in Fig. 2). Under these circumstances the cycloidal motion of the new-born ions does not come into play, i.e., these ions can be treated as unmagnetized in this region in contrast to the ambient protons and electrons which remain magnetized. Thus the exospheric ions can be thought of as forming a genuine beam (not a ring beam) in the sw reference frame, regardless of the cone angle α, continuously being pumped by ionization from the neutral gas background. This has considerable consequences on the features of the resulting low-frequency electromagnetic instabilities. Such a situation, to the knowledge of the authors, has not previously been subject to an instability analysis.

3. Low-Frequency Electromagnetic Instabilities

We consider a three-component plasma composed of the sw as the core plasma and a teneous unmagnetized beam of exospheric ions in relative drift ($\mathbf{v}_b = -\mathbf{v}_{sw}$) to the core. The beam propagates at an angle α to the IMF. Since the thermal velocities of both the exospheric ions and the sw protons are small against the sw (i.e., beam) velocity, it seems appropriate to ignore ion thermal effects in a first step, i.e., to treat both ion species as cold. The cold two-ion ideal Hall MHD plasma model includes the equations describing the proton dynamics

$$\frac{\partial n_p}{\partial t} + \nabla \cdot \left(n_p \varpi_p \right) = 0; \tag{2}$$

$$\frac{\partial}{\partial t}\left(n_p \varpi_p \right) + \nabla \cdot \left(n_p \varpi_p \varpi_p \right) = \frac{e n_p}{m_p}\left(\boldsymbol{E} + \varpi_p \times \boldsymbol{B} \right), \tag{3}$$

and the dynamics of the unmagnetized beam ions

$$\frac{\partial n_b}{\partial t} + \nabla \cdot \left(n_b \varpi_b \right) = 0; \tag{4}$$

$$\frac{\partial}{\partial t}\left(n_b \varpi_b \right) + \nabla \cdot \left(n_b \varpi_b \varpi_b \right) = \frac{e n_b}{m_b} \boldsymbol{E}. \tag{5}$$

The electrons are regarded as massless and cold so that the electric field $\boldsymbol{E}$ is given by,

$$\boldsymbol{E} = -\left(\varpi_e \times \boldsymbol{B} \right). \tag{6}$$

The displacement current is neglected, thus Ampere's law is

$$\frac{1}{\mu_0} \nabla \times \boldsymbol{B} = e\left(n_p \varpi_p + n_b \varpi_b - n_e \varpi_e \right). \tag{7}$$

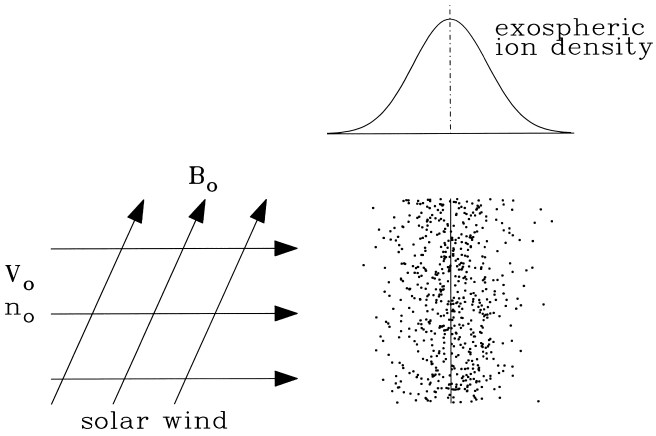

Fig. 2. Sketch of the interaction scenario: the sw penetrates the Phobos gas torus and interacts with a population of oxygen ions (indicated by the dots) continuously created by ionization from the neutral gas background. For scaling see Fig. 3.

The equations are closed with Faraday's law,

$$\frac{\partial \boldsymbol{B}}{\partial t} = -\nabla \times \boldsymbol{E}, \tag{8}$$

and the condition of quasineutrality,

$$n_e = n_p + n_b. \tag{9}$$

All notation is standard. When Eqs. (2)–(9) are linearized about a uniform state ($\mathbf{v}_e = \mathbf{v}_p = 0$, $\mathbf{v}_b = -\mathbf{v}_{sw}$, $n_e = n_p + n_b = n_0$, $\boldsymbol{B}_0$) and all quantities are assumed to vary as $\sim \exp(-i\omega t + i\boldsymbol{kr})$ we arrive after straightforward, but tedious, algebra at the dispersion relation

$$\left[\omega_b^2 \left[\frac{k_\parallel^2 c^2}{\omega_{pi}^2}\left(\omega^2 - \Omega_p^2 \right) + \frac{n_p}{n_b}\omega^2 \right] + \frac{m_p}{m_b}\frac{n_b}{n_e}\omega\left(\omega^2 - \Omega_p^2 \right)\left(\omega - k_\parallel v_{b\parallel} \right) \right]$$
$$\times \left[\omega_b \left[\frac{k^2 c^2}{\omega_{pi}^2}\left(\omega^2 - \Omega_p^2 \right) + \frac{n_p}{n_e}\omega^2 \right] + \frac{m_p}{m_b}\frac{n_b}{n_e}\left(\omega^2 - \Omega_p^2 \right) \right]$$
$$- \omega^2 \omega_b^3 \left(\omega^2 - \frac{n_b}{n_e}\Omega_p^2 \right) = 0 \tag{10}$$

where Ω_p is the proton gyrofrequency, ω is the frequency in the sw frame, $\omega_b = \omega - \boldsymbol{k}\mathbf{v}_b$ is the Doppler-shifted frequency in the beam (i.e., torus) reference frame and the subscript $\parallel$ indicates the direction along the undisturbed magnetic field. $\boldsymbol{k}$ may have any direction in the plane defined by $\boldsymbol{B}_0$ and $\mathbf{v}_b$. After factoring out $(\omega^2 - \Omega_p^2)$ Eq. (10) yields a polynomial of 7th order in ω which may exhibit one pair of complex conjugate solutions.

One may alternatively use the dielectric tensor approach to derive Eq. (10) and start from the cold dielectric tensor $\boldsymbol{K}(\omega)$ of a two-ion plasma with relative drift using an appropriate limit for low-frequency waves (see, for example, Sauer *et al.*, 1998). Then the dispersion relation results from the condition

$$\det\left|\boldsymbol{D}(\omega,\boldsymbol{k})\right| = 0 \tag{11}$$

where $\boldsymbol{D}$ is the dispersion tensor defined by

$$\boldsymbol{D}\cdot\boldsymbol{E} = \boldsymbol{k}\times(\boldsymbol{k}\times\boldsymbol{E}) + \frac{\omega^2}{c^2}\boldsymbol{K}\cdot\boldsymbol{E} \tag{12}$$

and $\boldsymbol{E}$ is the electric field associated with plasma fluctuations. This method provides the possibility to control the cold fluid calculations by introducing the more accurate kinetic version of the dielectric tensor in Eq. (11), which accounts for finite temperature effects such as wave-particle interaction. The strategy adopted here is to employ both models, i.e., we solve both the cold and the fully kinetic dispersion relation for a set of parameters we feel are appropriate for the Phobos-2 encounter with the neutral gas ring. The form of the kinetic version of the dielectric tensor used here is that of a collisionless, magnetized, electron-proton plasma with Maxwellian distribution functions (sw plasma) superimposed by the unmagnetized heavy ion beam, represented by a drifting Maxwellian distribution. A few comments on the kinetic approach are given in Appendix II. We used a value of the beam density two orders of magnitude below (2%) the background density $n_0 = 2$ cm^{-3} and assumed the beam ions to be singly ionized oxygen atoms with an atomic mass of 16. The assumed beam density is consistent with estimates of Dubinin *et al.* (1991) and Krymski *et al.* (1992). These authors calculated the expected oxygen ion density from a balance between ionization from the neutral gas torus and convective losses on the basis of an outgassing rate of $Q = 10^{23}$ s^{-1} for Phobos to be

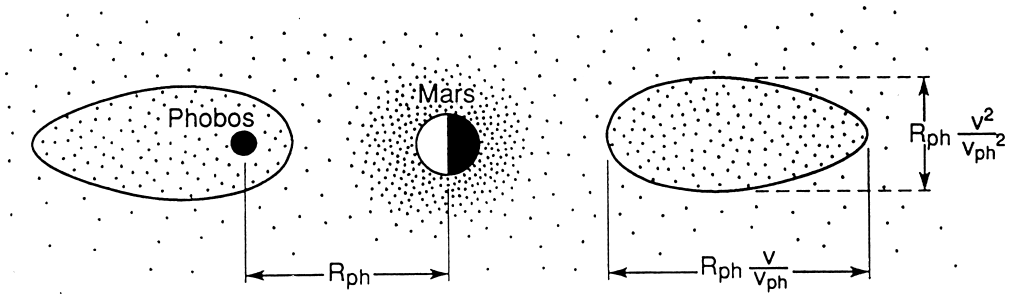

Fig. 3. The scenario for the neutral gas halo near Mars as calculated by Krymski *et al.* (1992) (their figure 1); $R_{ph} \sim 10^4$ km is the radius of the Phobos orbit, $v_{ph} \sim 2.6$ km/s is the orbital velocity of Phobos and $v \sim 0.2\ v_{ph}$ is the escape velocity of a neutral atom. The spatial extent of the oxygen gas torus is ~2000 km in radial direction and ~400 km in direction transverse to the orbital plane. The gyroradius of an oxygen ion is ~10^4 km (B = 3 nT).

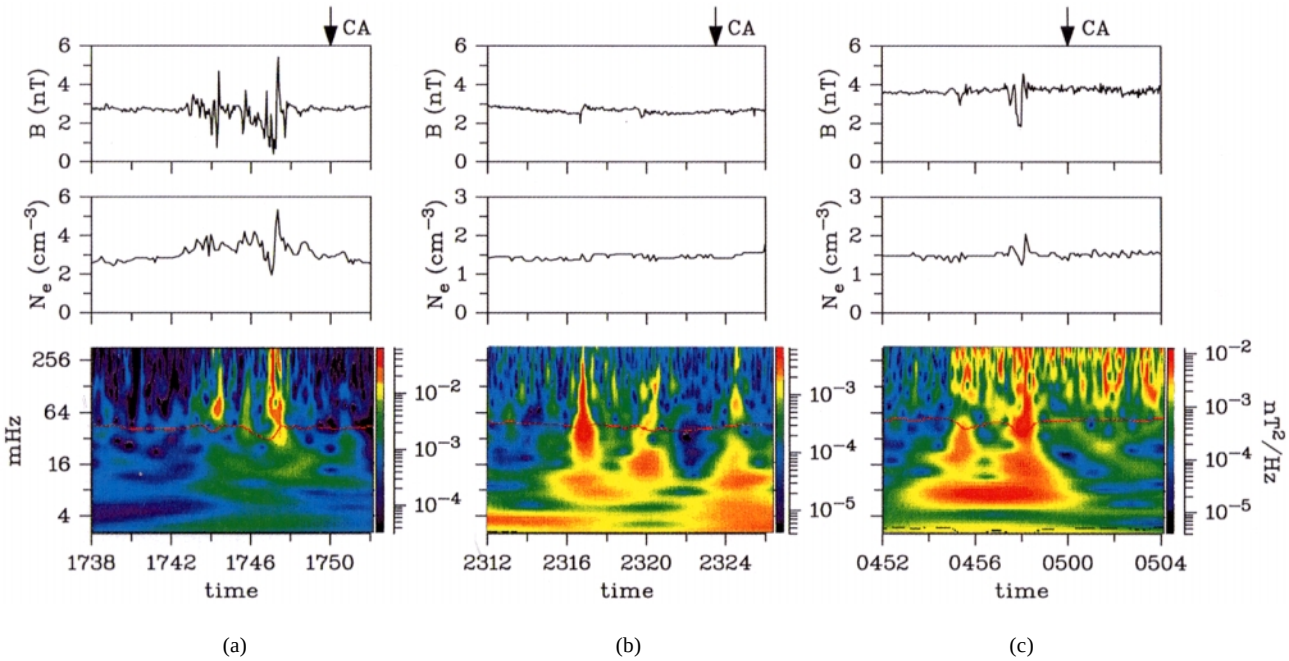

Fig. 4. Phobos events observed by the FGMM magnetometer aboard the Phobos-2 spacecraft during the first (a), the second (b) and the third (c) elliptical orbit (Feb. 1, 4, 8, 1989) on just before crossing the Phobos orbit. The arrow indicates the time of closest approach. The electron density records (middle panel) are from the PWS device. The bottom panel shows the low-frequency magnetic field power as a result of a wavelet analysis of the magnetic field turbulence. The proton cyclotron frequency is traced by a red line. Time labels are given in the format "hhmm"; a time difference of 2 min corresponds to a distance of ~300 km.

of the order of 0.01 cm^{-3}–0.1 cm^{-3} (see Appendix I). The scenario for the neutral gas halo is sketched in Fig. 3, taken from Krymski *et al.* (1992). We assume a cone angle $\alpha = 45°$ between the sw velocity vector and the IMF, typical for Mars. The sw flow speed is taken to have an Alfven Mach number $M_A = 8$. Figure 5 depicts the complex cold plasma dispersion for the modes of interest in which the real and imaginary parts of the frequency, normalized by Ω_p (top panel) and the normalized phase velocity and the beam frame frequency (bottom panel), are plotted as function of the wave number, normalized by c/ω_{pi}, at constant obliquity ($\theta = 10°$). As seen from this figure, the unstable mode arises from the coupling of the heavy ion beam to the whistler mode. The maximum growth rate is attained just adjacent to the threshold wavenumber for onset of the instability. The growth rate remains significant with growing wave number, accompanied by an approach of the beam frame frequency to zero, i.e., the wave may evolve into a nonoscillatory, almost purely growing mode in the beam frame. Figure 6 depicts the rate of the unstable mode growth maximized over the wave number as function of the propagation direction. With increasing obliquity, γ_{max} continuously increases and the maximum growth is shifted to higher real frequencies and wavenumbers. When approaching the limit of perpendicular propagation the frequency associated with maximum growth is beyond the regime where the electron mass can be ignored in cold plasma theory. The cold plasma theory, however, tends to yield exaggerated wave growth and kinetic effects due to finite temperature of the species are expected to mitigate the instability especially for higher wave numbers. In order to control the fluid results, warm plasma dipersion theory has been applied to the same situation where the electron and proton plasma beta have been set $\beta_e = \beta_p = 1$ (typical for the sw plasma). The velocity spread of the beam ions is not well known, we assume a relatively cold beam and adopt a value $\beta_b = 2(v_{th,b}/v_A)^2 = 0.01$. Figures 7 and 8 depict warm plasma dispersion results for the same parameters as in Figs. 5 and 6. It is seen from Fig. 7 that thermal effects do not completely "smear out" the instability but confine the wave growth to a narrow wave number range confirming the resonant character of the instability. A remarkable modification brought about by the warm plasma theory is displayed in Fig. 8. The wave growth is seen to be confined to a range of propagation directions close to parallel, in contrast to the predictions of the cold

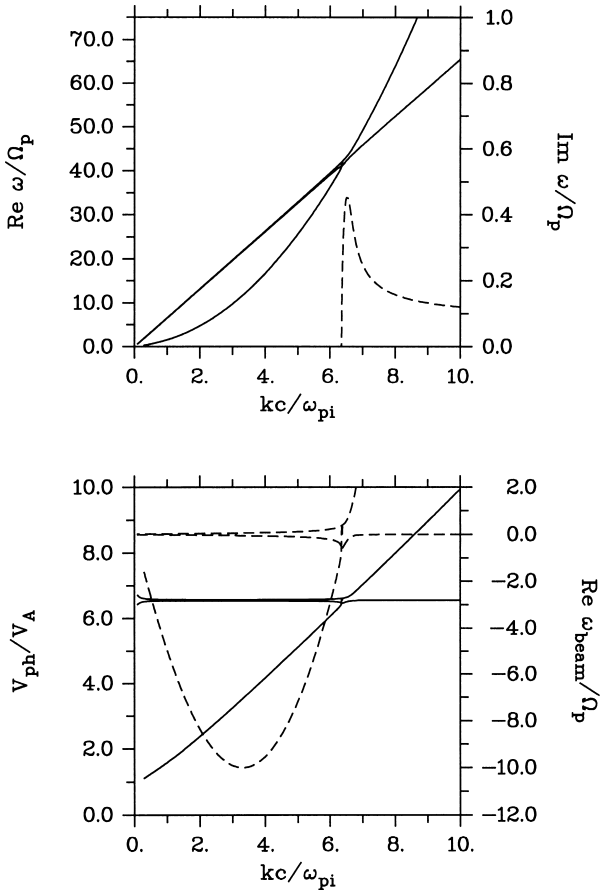

Fig. 5. Cold plasma dispersion diagram for electromagnetic waves in the whistler range of frequencies in the sw plasma coexisting with a beam of oxygen ions whose velocity vector $\mathbf{v}_b = -\mathbf{v}_{sw}$ is 45° inclined to the IMF and whose density is 2% of the ambient sw density. The wave vector $\boldsymbol{k}$ is in the $\mathbf{v}_b$-$\boldsymbol{B}_0$-plane "between" the vectors $\mathbf{v}_b$ and $\boldsymbol{B}$ and makes an angle of 10° to the magnetic field direction. Top panel: real part (solid lines) and imaginary part (dashed lines) of the frequency, normalized by the proton cyclotron frequency Ω_p, versus wave number, normalized by the proton inertial length c/ω_p.Bottom panel: phase velocity in the sw frame normalized by the Alfven velocity (solid lines) and real frequency in the beam frame (dashed lines) versus wave number. The unstable mode is the right-hand part of the beam mode.

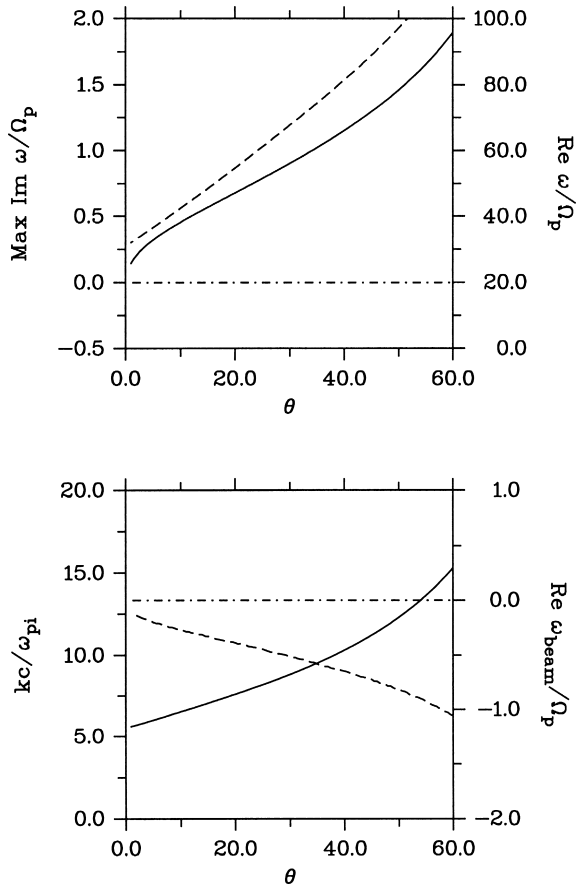

Fig. 6. Top panel: Cold plasma growth rate maximized over wave number (solid) and associated real frequency in the sw frame (dashed) versus propagation angle θ. Bottom panel: Wave number (solid) and real frequency in the beam frame (dashed) for maximum growth versus θ.

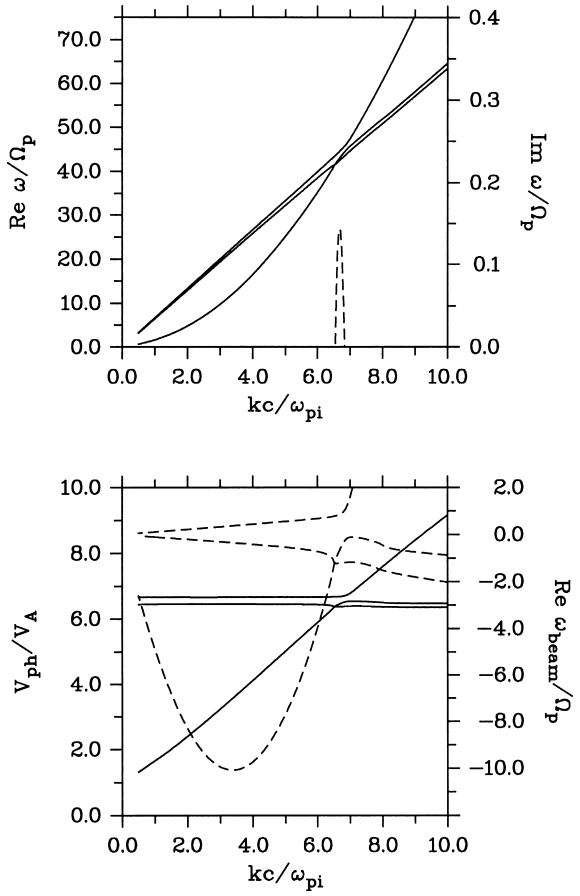

Fig. 7. The same as Fig. 5, here calculated using the fully kinetic dielectric tensor for the three component plasma. Additional parameters are $\beta_e = \beta_p = 1$, $\beta_b = 0.01$ where $\beta_\alpha = (v_{th,\alpha})^2/2v_A^2$.

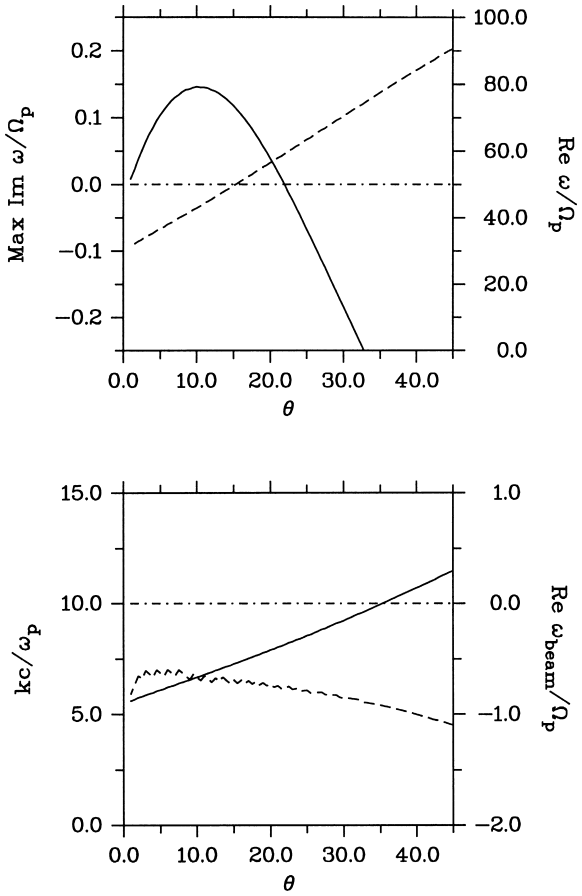

Fig. 8. The same as Fig. 6, here as predicted by warm plasma theory.

plasma theory. Variation of the obliquity shows a maximum of the growth rate γ_{max} at an angle as small as 10°.

Unlike several ring-beam ion/ion instabilities which predict that the most unstable mode propagates parallel to the magnetic field, the relevant mode here is stable for parallel propagation but aquires large growth rates at relatively large wavenumbers ($kc/\omega_{pi} \sim 5$) and real frequencies ($\omega/\Omega_p \sim 30$) for propagation oblique to $\boldsymbol{B}_0$. In order to understand the physical nature of this instability we recall that in the general case a magnetized beam particle (e.g., a pick up ion) can resonate with a wave when its velocity along $\boldsymbol{B}$ is sufficient to Doppler shift the wave frequency to some integral multiple ($n = 0, \pm1, \pm2, ...$) of the beam particle gyrofrequency Ω_b,

$$\omega - \boldsymbol{k}\varpi_b + n\Omega_b \approx 0. \tag{13}$$

An unmagnetized beam ion can only resonate with the wave via the $n = 0$ resonance, $\omega - \boldsymbol{k}\boldsymbol{v}_b \approx 0$, which requires that its velocity is close to the wave phase velocity along the beam. Figures 5 and 7 give evidence that this condition is satisfied, showing that the instability sets in where the beam directed phase velocity intersects the beam velocity. Since the beam propagates at a velocity of several times the Alfven velocity, the whistler mode is the most likely candidate to meet this requirement. In order to provide a mechanism for wave particle interaction in such case, the wave electric field is required to possess longitudinal field components. This is the case since oblique electromagnetic modes yield density fluctuations. The maximum growth at a finite obliquity can thus be understood as the result of a balance between the increase with θ of both the compressive nature of the wave and the Landau-type whistler damping. It comes as a surprise, however, that the sw protons seem to be involved in the instability as suggested by Figs. 5 and 7. From the bottom panel of these figures it is seen that the unstable wave satisfies near maximum growth

$$\omega - \boldsymbol{k}\varpi_b + \Omega_p \approx 0, \tag{14}$$

i.e., maximum growth is associated with a beam (≈space craft) frame frequency close to $\omega_b \approx -\Omega_p$. The unstable wave is almost right-hand circularly polarized in the sw frame, but due to the Doppler shift the wave appears as left-hand polarized in the beam frame. The growth rate is insensitive to the proton temperature and does not depend much on the mass of the beam ions, but the beam density, the velocity spread of the beam ions and the electron temperature appear to control the instability. We emphasize that the beam ions make a dominant contribution to the mass density perturbation associated with the unstable wave. With the help of the linearized continuity and momentum equations of the beam ions and Faraday's law the mass density perturbation can be expressed in terms of the transverse wave magnetic field amplitude

$$\frac{\delta\rho}{\rho_0} = \frac{n_b}{n_0}\frac{i\omega\Omega_p}{\left(\omega - \boldsymbol{k}\varpi_b\right)^2}\tan\theta\frac{\delta B_y}{B_0}, \qquad (15)$$

with $\rho_0 = n_p m_p + n_b m_b \approx n_p m_p$. The square of the beam frame frequency in the denominator of Eq. (15) may compensate the small equilibrium density of the beam ions to yield a mass density perturbation of the same order as the relative magnetic field perturbation. Thus, though their high real frequency in the sw frame the whistler instability may strongly contribute to the heavy ion dynamics and cause structuring of the beam ions. If the $\boldsymbol{k}$-vector is allowed to also have components out of the $\mathbf{v}_b$-$\boldsymbol{B}_0$-plane, no new maxima of the growth rate are created. Several features of this instability can also be found among the various unstable propagating waves predicted by kinetic theory in the presence of a ring-beam distribution, and it was pointed out by Brinca and Tsurutani (1987) and later in other studies (Goldstein *et al.*, 1990) that wave modes with maximum growth slightly away from parallel propagation and highly elliptical or linear polarization, and even non-oscillatory structures, can be excited by pickup ions. While in these studies maximum growth rates of the order of a fraction of the heavy ion gyrofrequency emerged, favoured by a cold (monoenergetic) ring beam, the instability considered here exhibits growth rates of the order of a fraction of the proton gyrofrequency, i.e., at least an order of magnitude higher. The intense wave growth, coexisting with a preference of the proton cyclotron frequency in the beam frame, maximum growth at small obliquities and beam ion mass density perturbations are the distinguishing features of the instability. The question arises as to what extent the characteristics of the instability depend on the model parameters adopted for the calculation. Whereas the solar wind parameters (cone angle α, density, Mach number, electron and proton temperatures) are typical background values, the influence of the beam parameters (density, velocity spread) is of interest. As is expected, a decrease in the beam density is associated with a reduction of the maximum growth rate and the corresponding obliquity. A beam density $n_b/n_0 = 0.005$, four times less than the nominal value, appears as a threshold for the instability. This suggests a lower limit of the Phobos outgassing rate ($Q > 2.5 \times 10^{22}$ s^{-1}) for the sw interaction with the gas torus to produce observable features. The modifications brought about by an increase in the velocity spread of the beam ions go in the same direction. A four times higher β_b ($\beta_b = 0.04$) is sufficient to "smear out" the instability.

We should point to the fact, that there is another unstable region for small wavenumbers $kc/\omega_p \leq 0.1$, associated with a second intersection of the whistler phase velocity with the beam velocity. It results from the fact that the whistler branch approaches a finite frequency (Ω_p) in the $k = 0$ limit in the presence of an unmagnetized ion beam, which implies a singularity of the phase velocity in this limit (see Sauer *et al.*, 1998). This long wavelength instability, however, is not on the focus of this study.

4. Comparison with Observations

Two features of the Phobos events are crucial for a comparison with theory: (1) The fact that the events observed during each of the three orbits are composed of two narrow regions of more or less enhanced perturbations, separated by a period of ~3 min, and (2) the enhanced low-frequency wave activity around the proton gyrofrequency Ω_p seen in the bottom panels of Figs. 4(a)–(c). The results of the instability theory allow at least a qualitative approach to these observational features. As far as the spectrum of the low-frequency oscillations is concerned, the dispersion diagrams in Figs. 5 and 7 clearly indicate that the maximum rate of growth is associated with a real frequency close to Ω_p in the beam frame and that wave growth is also predicted for the whole frequency interval $0 \leq |\omega_b| \leq \Omega_p$, consistent with the observations. With respect to the double structure of the events we should note that the wavelength associated with maximum growth is a characteristic spatial scale provided by the instability theory which may serve for a comparison. Assuming that the events represent an almost standing structure in the torus frame, the time difference $\Delta t = 3$ min corresponds to a distance of $\Delta t \times v_{sp} = 180\text{ s} \times 2.5\text{ km/s} = 450$ km along the spacecraft orbit ($v_{sp} \approx 2.5$ km/s is the spacecraft velocity). A wave number at maximum growth of $kc/\omega_{pi} \approx 5$ (Figs. 5 and 7) corresponds to a wavelength $\lambda \approx 1.25 \times c/\omega_{pi} = 1.25 \times 160$ km = 200 km along the direction of propagation of the fastest growing mode, i.e., 10° off the magnetic field direction towards the sw flow direction. Since the spacecraft crosses the Phobos orbit almost perpendicular to the sw flow direction (Fig. 1) it "sees" this structure at an angle $\psi \approx 55°$ (sum of the cone angle $\alpha \approx 45°$ and the angle of maximum growth), resulting in an enlarged wavelength $\lambda/\cos\psi \approx 350$ km closer to the observed distance.

5. Discussion

It has been known for long time from studies of the sw interaction with cometary atmospheres that a magnetized plasma stream can interact in more than one way with secondary ions injected from a source region into this stream and that the way in which they interact changes with the direction of the magnetic field relative to the flow direction. In this study an interaction mechanism is isolated and examined in the framework of a linear instability theory, which seems to provide an explanation of the Phobos events in terms of an ion beam instability operating in the region of a putative gas torus around the Phobos orbit which is maintained by outgassing of the Martian moon. This instability is "reactive" in nature, operates at the cost of the kinetic energy of the beam ions transverse to the ambient magnetic field and exhibits maximum growth slightly away ($\theta \sim 10°$) from parallel propagation with real frequencies well above the proton gyrofrequency Ω_p in the sw frame (corresponding to frequencies around Ω_p in the beam frame) and wavenumbers $kc/\omega_{pi} \sim 5$. We suggest that this instability might bring about observable features. Elements of this instability seems to contribute also to unstable wave generation in the presence of a ring-beam ion distribution. In order to allow for a linear stability analysis, a simplified model of the plasma and geometric conditions during the encounter has been introduced which assumes the interaction region as uniform and treates the newly created ions as a beam in the sw frame whose density reaches a fraction (≈2%) of the

ambient plasma density. At a first glance, this zero order state (which is the object of the instability analysis) seems not be well-posed because an ion beam can coexist in a magnetized plasma only if it propagates along the magnetic field. Nevertheless, the presence of a localized source of ions in a magnetized plasma flow can establish a situation to which this approximation can be applied. Provided the created ions do not carry out a complete gyration in the region of interest, the emission region can be thought of as a source for a beam in the above sense. In a certain sense, this situation can be considered as a particular case of a non-gyrotropic ion distribution. The cold plasma approximation stresses the fluid character of the resulting instability and yields exaggerated growth rates. A treatment in the framework of the Vlasov-Maxwell theory reveals, that although the growth rates are significantly reduced for large wave numbers, the instability is not "smeared out" completely by finite temperature effects such as Landau and cyclotron damping, and maximum growth rates of the order of a fraction of the proton gyrofrequency still emerge. A limitation of the stability analysis is that it concentrates on wave growth in time under homogeneous conditions rather than spatial wave amplification. The latter would be more realistic since the interaction region is limited in size and the question may arise as to whether the spatial extent of the Phobos gas torus is sufficient to allow for an amplification of the unstable wave to observable amplitudes. Spatial and temporal growth of a wave along the ray path is known to be linked by the group velocity, $Jm(k) \sim -Jm(\omega)/v_{gr}$. Since the mode changes from whistler-like to beam-like within the region of instability, the group velocity in the beam frame is small which stretches the convective growth time and supports the formation of measurable amplitudes. Another serious limitation imposed by the linear stability analysis is that the saturated state of the instability can not be assessed. To give at least an idea of what the saturated state may look like, we refer to the 1D hybrid code simulations of Omidi and Winske (1987) of sw massloading by an extended neutral gas profile. They found in the "oblique" case ($30° < \alpha < 70°$) that nearly sinusoidal waves grow in the initial stage which eventually steepen and saturate. A direct comparison with our results is not possible since the limitation imposed by the one-dimensionality implies that the cone angle always coincides with the angle between $\boldsymbol{k}$ and $\boldsymbol{B}_0$; i.e., the simulations do in general not cover the propagation direction of maximum growth.

In this context we would like to point finally to an observation during the Phobos mission that is not directly related to the Phobos events. Russell *et al*. (1990) reported on a persistent but weak signal at the proton gyrofrequency detected in the region about 2–3R_M in front of Mars. It was found to correspond to a left-hand elliptically polarized wave propagating at a small to moderate angle to the magnetic field and was suggested to be associated with the pick-up of newly ionized hydrogen atoms. It is tempting to speculate that this signal results from the above instability because its properties just coincide with those predicted for the fastest growing mode under the conditions realized near Mars. Moreover, we suggest, that this instability comes into play not only in cases of a spatially limited neutral gas cloud but in any situation where the sw interacts with a relatively weak and homogeneous heavy ion source, e.g., at large distances from a comet or in the late stage of an AMPTE release (see, e.g., Sauer *et al*., 1998).

In summary, in spite of the limitations of the model used in this study, we feel that the approach provides further insight into the interpretation of the Phobos events and introduces a mechanism which is likely to be capable of explaining these unique observations.

Acknowledgments. The authors wish to express their gratitude to the International Space Science Institute (ISSI) at Bern for their support of the collaboration in the framework of the Visiting Science Programme.

This work was supported by the Max-Planck-Gesellschaft zur Förderung der Wissenschaften e.V., Berlin.

Appendix I

The estimates of Dubinin *et al*. (1991) and Krymski *et al*. (1992) of the expected oxygen ion density within the Phobos gas torus start from the assumption that the neutral atoms initially expand freely from the Phobos surface, but that the gravitational field of Mars very rapidly begins to have an effect and will soon bind the majority of the atoms, thereby preventing their free expansion. The extension of the neutral gas torus along the plane of the Phobos orbit can be estimated to be $\sim 2 \times 10^3$ km whereas transverse to the plane, the dimension of the torus is approximately 400 km. For comparison, the gyroradius of an oxygen ion in an interplanetary magnetic field of 3 nT is 10^4 km. The average neutral gas density can be estimated to be $n_N = Q\tau_{loss}/V_t \approx 4 \times 10^3$ cm^{-3} where V_t is the torus volume and $\tau_{loss} \sim 10^6$ s is the characteristic time for neutral losses from the gas torus. Taking into account that the newborn ions will only be within the gas torus at the initial stage of their gyration motion and assuming an ionization time of 10^6 s results in an estimate of the number density of the heavy ions within the gas torus of $n_b \approx 0.01$–0.1 cm^{-3}.

Appendix II

Following the notation of Gary (1993), in a reference frame whose z-axis lies along $\boldsymbol{B}_0$ and the $\boldsymbol{k}$-vector, forming an angle θ with $\boldsymbol{B}_0$, is contained in the x-z-plane, the components D_{ik} of the dispersion tensor of a plasma composed of a number of species (subscript α) can be written

$$
\begin{aligned}
D_{11} &= \omega^2 - k_\parallel^2 c^2 + \sum_\alpha \omega_{p\alpha}^2 S_{11,\alpha} \\
D_{12} &= \sum_\alpha \omega_{p\alpha}^2 S_{12,\alpha} \\
D_{22} &= \omega^2 - k^2 c^2 + \sum_\alpha \omega_{p\alpha}^2 S_{22,\alpha} \\
D_{13} &= -k_\parallel k_\perp c^2 + \sum_\alpha \omega_{p\alpha}^2 S_{13,\alpha} \\
D_{23} &= \sum_\alpha \omega_{p\alpha}^2 S_{23,\alpha}
\end{aligned}
\qquad \text{(A1)}
$$

$$D_{33} = \omega^2 - k_\perp^2 c^2 + \sum_\alpha \omega_{p\alpha}^2 S_{33,\alpha}$$

where $\omega_{p\alpha}$ is the species plasma frequency (α = e, p, b in our case) and $S_{mn,\alpha}$ are dimensionless quantities. The contributions $S_{mn,\alpha}$ from a magnetized particle species with Maxwellian distribution function are given by

$$S_{11,\alpha} = \zeta_0^\alpha \sum_n \frac{n^2}{\mu_\alpha} \Lambda_n(\mu_\alpha) Z(\zeta_n^\alpha)$$

$$S_{12,\alpha} = i\zeta_0^\alpha \sum_n n\Lambda_n'(\mu_\alpha) Z(\zeta_n^\alpha)$$

$$S_{22,\alpha} = \zeta_0^\alpha \sum_n \left[-2\mu_\alpha \Lambda_n'(\mu_\alpha) + \frac{n^2}{\mu_\alpha} \Lambda_n(\mu_\alpha) \right] Z(\zeta_n^\alpha) \tag{A2}$$

$$S_{13,\alpha} = \mathrm{sign}(e_\alpha) \zeta_0^\alpha \sum_n \frac{n}{\sqrt{2\mu_\alpha}} \Lambda_n(\mu_\alpha) Z'(\zeta_n^\alpha)$$

$$S_{23,\alpha} = -\mathrm{sign}(e_\alpha) i\zeta_0^\alpha \sum_n \sqrt{\frac{\mu_\alpha}{2}} \Lambda_n'(\mu_\alpha) Z'(\zeta_n^\alpha)$$

$$S_{33,\alpha} = -\zeta_0^\alpha \sum_n \Lambda_n(\mu_\alpha) \zeta_n^\alpha Z'(\zeta_n^\alpha)$$

with $S_{21,\alpha} = -S_{12,\alpha}$, $S_{32,\alpha} = -S_{23,\alpha}$, $S_{31,\alpha} = S_{13,\alpha}$, $\zeta_n{}^\alpha = (\omega + n\Omega_\alpha)/\sqrt{2}\, k_\parallel v_{th,\alpha}$, $\Lambda_n(x) = e^{-x} I_n(x)$, $\Lambda_n'(x) = e^{-x}[I_n'(x) - I_n(x)]$, $\mu_\alpha = (k_\perp v_{th,\alpha}/\Omega_\alpha)^2$. The gyrofrequency $\Omega_\alpha = e_\alpha B/m_\alpha$ is defined as positive for ions and negative for electrons. ω is the wave frequency, the subscripts $\parallel$, $\perp$ indicate the directions along and perpendicular to $\boldsymbol{B}_0$, and $v_{th,\alpha}$ is the species thermal velocity. I_n is the Besselfunction of n-th order and Z is the plasma dispersion function. The contributions $S_{mn,b}$ from the unmagnetized heavy beam ions, represented by a drifting Maxwellian, can be written

$$S_{11,b} = \xi Z(\eta)\cos^2\theta - \xi^2 Z'(\eta)\sin^2\theta - \frac{k v_{b\perp}}{\omega} \xi^2 Z'(\eta)\sin\theta\cos\theta,$$

$$S_{12,b} = 0,$$

$$S_{22,b} = \xi Z(\eta),$$

$$S_{13,b} = -\left[\xi Z(\eta) + \xi^2 Z'(\eta)\right]\sin\theta\cos\theta - \frac{k v_{b\perp}}{\omega} \xi^2 Z'(\eta)\cos^2\theta, \tag{A3}$$

$$S_{31,b} = -\left[\xi Z(\eta) + \xi^2 Z'(\eta)\right]\sin\theta\cos\theta + \frac{k v_{b\perp}}{\omega} \xi^2 Z'(\eta)\sin^2\theta,$$

$$S_{23,b} = S_{32,b} = 0,$$

$$S_{33,b} = \xi Z(\eta)\sin^2\theta - \xi^2 Z'(\eta)\cos^2\theta - \frac{k v_{b\perp}}{\omega} \xi^2 Z'(\eta)\sin\theta\cos\theta,$$

where $\xi = \omega/\sqrt{2}\, k v_{th,b}$, $\eta = (\omega - \boldsymbol{k}\cdot\mathbf{v}_b)/\sqrt{2}\, k v_{th,b}$, and $\mathbf{v}_{b\perp}$ is the component of the beam drift velocity transverse to $\boldsymbol{k}$. Note that $S_{13,b} \neq S_{31,b}$. These expressions can be derived from the dielectric tensor components of a magnetic field-free, warm, plasma in the presense of a particle drift in a $\boldsymbol{k}$-oriented frame of reference (z-axis along $\boldsymbol{k}$), given, for example by Melrose (1986).

References

Baumgärtel, K. and K. Sauer, Interaction of a magnetized plasma stream with an immobile ion cloud, *Ann. Geophys.*, **10**, 763–771, 1992.

Baumgärtel, K. and K. Sauer, Bi-ion fluid description of plasma dust interaction: relevance to Phobos events, *Adv. Space Res.*, **13**, (10)291–294, 1993.

Baumgärtel, K., K. Sauer, A. Bogdanov, E. Dubinin, and M. Dougherty, 'Phobos Events': signature of solar wind dust interaction, *Planet. Space Sci.*, **44**, 589–601, 1996.

Bogdanov, A. V., Mars satellite Deimos interaction with the solar wind and its influence on flow around Mars, *J. Geophys. Res.*, **86**, 6921–6932, 1981.

Brinca, A. L., Cometary linear instabilities: From profusion to prospective, in *Cometary Plasma Processes*, pp. 211–222, Geophysical Monograph 61, American Geophysical Union, 1991.

Brinca, A. L. and B. T. Tsurutani, On the polarization, compression and nonoscillatory behaviour of hydromagnetic waves associated with pickup ions, *Geophys. Res. Lett.*, **14**, 495–498, 1987.

Dubinin, E. M., The Phobos and Deimos effects, *Adv. Space Res.*, **13**, (10)271–290, 1993.

Dubinin, E. M., R. Lundin, N. F. Pissarenko, S. V. Barabash, A. V. Zakharov, H. Koskinen, K. Schwingenschuh, and Ye. G. Yeroshenko, Indirect evidence for a gas/dust torus along the Phobos orbit, *Geophys. Res. Lett.*, **17**, 861–864, 1990.

Dubinin, E. M., N. F. Pissarenko, S. V. Barabash, A. V. Zakharov, R. Lundin, R. Pellinen, K. Schwingenschuh, and Ye. G. Yeroshenko, Plasma and magnetic field effects associated with Phobos and Deimos tori, *Planet. Space Sci.*, **39**, 113–121, 1991a.

Dubinin, E. M., N. F. Pissarenko, S. V. Barabash, A. V. Zakharov, R. Lundin, H. Koskinen, K. Schwingenschuh, and Ye. G. Yeroshenko, Tails of Phobos and Deimos in the solar wind and in the Martian magnetosphere, *Planet. Space Sci.*, **39**, 123–130, 1991b.

Dubinin, E. M., R. Lundin, K. Schwingenschuh, and R. Grard, Some features of the Martian bow shock, *Adv. Space Res.*, **15**, (8/9), 423–431, 1995.

Gary, S. P., *Theory of Space Plasma Microinstabilities*, p. 143, Cambridge University Press, Cambridge, 1993.

Goldstein, M. L., H. K. Wong, and K. H. Glassmeier, Generation of low-frequency waves at comet Halley, *J. Geophys. Res.*, **95**, 947–955, 1990.

Horanyi, M., J. A. Burns, M. Tatrallyay, and J. G. Luhmann, Toward understanding the fate of dust lost from the Martian satellites, *Geophys. Res. Lett.*, **17**, 853–856, 1990.

Ip, W.-H. and M. Banaskiewicz, On the dust/gas tori of Phobos and Deimos, *Geophys. Res. Lett.*, **17**, 857–860, 1990.

Ishimoto, H. and T. Mukai, Phobos dust rings, *Planet. Space Sci.*, **42**, 691–697, 1994.

Kholshevnikov, K. V., A. V. Krivov, L. L. Sokolov, and V. B. Titov, The dust torus around Phobos orbit, *ICARUS*, **105**, 351–362, 1993.

Krivov, V. A. and D. P. Hamilton, Martian dust belts: waiting for discovery, *ICARUS*, **128**, 335–353, 1997.

Krymski, A. M., T. K. Breus, M. K. Dougherty, D. J. Southwood, and W. I. Axford, The electromagnetic effects of the solar wind interaction with the Phobos neutral gas halo and dust torus, *Planet. Space Sci.*, **40**, 1033–1041, 1992.

Melrose, D. B., *Instabilities in Space and Laboratory Plasmas*, p. 20, Cambridge University Press, Cambridge, 1986.

Mendis, D. A. and W. I. Axford, Satellites and magnetospheres of outer planets, *Ann. Rev. Earth Planet. Sci.*, **2**, 419–474, 1974.

Omidi, N. and D. Winske, A kinetic study of solar wind mass loading and cometary bow shocks, *J. Geophys. Res.*, **92**, 13,409–13,426, 1987.

Riedler, W., D. Möhlmann, V. N. Oraevski *et al.*, Magnetic fields near Mars, *Nature*, **341**, 604–607, 1989.

Russell, C. T., J. G. Luhmann, K. Schwingenschuh, W. Riedler, and Ye.

G. Yeroshenko, Upstream waves at Mars: Phobos observations, *Geophys. Res. Lett*., **17**, 897–900, 1990.

Sauer, K., K. Baumgärtel, and U. Motschmann, Phobos events as precursors of solar wind-dust interaction, *Geophys. Res. Lett*., **20**, 165–168, 1993.

Sauer, K., E. Dubinin, K. Baumgärtel, and A. Bogdanov, Deimos—an obstacle to the solar wind, *Science*, **269**, 1075–1078, 1995.

Sauer, K., E. Dubinin, K. Baumgärtel, and V. Tarasov, Low-frequency electromagnetic waves and instabilities within the Martian bi-ion plasma, *Earth Planets Space*, **50**, 269–278, 1998.

Soter, S., The dust belts of Mars, Cornell Center for Radiophys. and Space Phys., Rep. No. 462, 1971.

Thorne, R. M. and B. T. Tsurutani, Resonant interactions between cometary ions and low frequency electromagnetic waves, *Planet. Space Sci*., **35**, 1501–1511, 1987.

Tsurutani, B. T., Comets: a laboratory for plasma waves and instabilities, in *Cometary Plasma Processes*, pp. 189–209, Geophysical Monograph 61, American Geophysical Union, 1991.

Wu, C. S. and R. C. Davidson, Electromagnetic instabilities produced by neutral particle ionization in interplanetary space, *J. Geophys. Res*., **72**, 5399–5406, 1972.

K. Baumgärtel (e-mail: kbaumgaertel@aip.de), K. Sauer (e-mail: sauer@linax1.mpae.gwdg.de), E. Dubinin (e-mail: dubinin@linax1.mpae.gwdg.de), V. Tarrasov (e-mail: vtarasov@isr.lviv.ua), and M. Dougherty (e-mail: m.dougherty@ic.ac.uk)